



# Iron and oxygen isotope systematics during corrosion of iron objects: a first approach

Thomas Rose<sup>1,2,3</sup> · Philippe Télouk<sup>4</sup> · Jens Fiebig<sup>1</sup> · Horst R. Marschall<sup>1,6</sup> · Sabine Klein<sup>5,6</sup>

Received: 20 July 2019 / Accepted: 23 April 2020  
© Springer-Verlag GmbH Germany, part of Springer Nature 2020

## Abstract

Iron objects are among the most abundant type of metal artefacts in the archaeological record and help to deepen our understanding of past societies and their technologies. However, sampling of them is often problematic due to the destructive character of most analytical methods. In this study, iron and oxygen isotope compositions of iron artefacts from marine and water under-saturated oxidising environments were analysed in a first attempt to gather artefact information from the corrosion layer without sampling the object directly. No Fe isotope fractionation between artefact and its corrosion products was recognised for both environments but cannot be excluded for marine environments. Hence, the artefact's Fe isotope composition can be determined from the corrosion layer. This allows the characterisation of artefacts which cannot be sampled directly. Because the available data precluded a clear identification of the underlying processes, possible fractionation mechanisms resulting in this situation are presented. Furthermore, the results of this study indicate that corrosion products have the same oxygen isotope composition as their source water. As for marine corrosion, general absence of oxygen isotope fractionation could not be manifested here, because only a small sample size was available for the present study. However, a complex interplay of many parameters governs the oxygen isotope compositions of corrosion products on metallic iron. Especially oxidising environments above the water table have a strong impact on the oxygen isotope composition of the corrosion layer. The first-order controlling mechanisms, such as evaporation, are set by the local environment and cannot be reconstructed. Therefore, the oxygen isotope composition of corrosion products seems to bear no valuable potential for archaeometallurgical research.

**Keywords** Iron isotopes · Oxygen isotopes · Atmospheric corrosion · Marine corrosion · Rust

## Introduction

Iron objects constitute one of the most frequently recovered types of metal artefacts and, therefore, have been extensively

investigated analytically to gain information about past societies (e.g. Baron et al. 2011; Dillmann et al. 2017; Joosten et al. 1998; Pleiner 2000). Several scientific approaches were developed to trace the ore provenance of the objects (Charlton 2015), most promising among them is trace element analysis of slag inclusions (Blakelock et al. 2009; Coustures et al. 2003; Desaulty et al. 2009; Dillmann and L'Héritier 2007; Leroy et al. 2012; L'Héritier et al. 2016) and osmium isotopes (Brauns et al. 2013; Brauns et al. 2020; Dillmann et al. 2017). Recently, iron isotopes were suggested as an additional tool (Milot et al. 2016; Rose et al. 2019). All of these methods require destructive sampling. However, destructive sampling of these artefacts, even only on the micro-scale, is often unwanted or limited due to the partially unique character of the objects. This difficulty could be overcome if valuable information about the provenance could be extracted from the corrosion layer as it is already done in metallography by studying remnant structures to gain information about the carbon content and the production process (e.g. Notis 2002; Stepanov et al. 2018). In

✉ Thomas Rose  
thomas.rose@daad-alumni.de

<sup>1</sup> Institut für Geowissenschaften, Goethe Universität, Altenhöferallee 1, 60438 Frankfurt am Main, Germany  
<sup>2</sup> Department of Bible, Archaeology and Ancient Near East, Ben-Gurion University of the Negev, Be'er Sheva, Israel  
<sup>3</sup> Department of Antiquity, Sapienza University of Rome, Rome, Italy  
<sup>4</sup> Univ Lyon, ENS-Lyon, Université Lyon, Lyon, France  
<sup>5</sup> Forschungsbereich Archäometallurgie, Deutsches Bergbau-Museum Bochum, Am Bergbaumuseum 31, 44791 Bochum, Germany  
<sup>6</sup> FIERCE, Frankfurt Isotope & Element Research Center, Goethe Universität, Altenhöferallee 1, 60438 Frankfurt am Main, Germany

combination with the high abundance and large number of iron artefacts in the archaeological record, this would allow large-scale studies without damaging the objects directly.

### Corrosion of iron objects

The basic principle of iron corrosion is the formation of a galvanic cell, as soon as iron gets in contact with water. Simultaneous oxidation of iron to aqueous Fe(II) (Eq. 1) and reduction of dissolved molecular oxygen (DMO) in water to hydroxide ions (Eq. 2) lead to the formation of relatively unstable ferrous hydroxides (Eq. 3) (Selwyn et al. 1999; Park and Dempsey 2005):



In marine environments at low oxygen levels, this relatively unstable compound may precipitate and can undergo partial oxidation to Fe(II)–Fe(III) compounds (green rust), which finally will transform to magnetite. At high DMO levels and pH > 6, ferrous iron will be completely oxidised to ferric hydroxide produced according to Eq. 3, which will precipitate and slowly transform into goethite. During the transformation to magnetite and goethite, a part of the water is released. At high DMO levels and low pH, Fe(II) ions remain in the solution. The resulting corrosion layer grows with time and spatially separates both reactions, limiting the diffusion of DMO to the metal surface (Selwyn et al. 1999).

In marine environments, corrosion carries on because the magnetite layer allows the transfer of electrons from the anodic reaction site at the metal-magnetite interface to the cathodic reaction site at the sediment/water-magnetite interface (Selwyn et al. 1999). The water at the anodic reaction site turns into a local electrolyte with (strongly) reduced concentrations of DMO and higher concentrations of anions. Among them, chlorides are the most abundant and can easily diffuse into the electrolyte due to their high mobility. They balance the charges in all further reactions proceeding in the electrolyte and therefore catalyse the corrosion process (Gerwin and Baumhauer 2000; Bellot-Gurlet et al. 2009; Selwyn and Argyropoulos 2013). Hydrolysis of aqueous Fe(II) in the electrolyte leads to the production of Fe(OH)<sup>+</sup> and H<sup>+</sup> ions. The latter lower the pH of the electrolyte and promote further hydrolysis of water. Due to the low pH, Fe(II) ions cannot precipitate and corrosion would continue until all iron is converted into corrosion products. However, these reactions are controlled by the reduction of DMO at the magnetite-sediment/water interface, which consumes the electrons released during the oxidation of iron. The hydroxide ions will react with the

magnetite layer or any dissolved iron compound in it to non-conductive goethite, preventing any further interaction between DMO and the magnetite. This reaction and the burial environment are highly likely to strongly reduce the corrosion rate (Selwyn et al. 1999; Memet 2007; Saheb et al. 2010).

Between the magnetite layer and the metal surface akaganeite ( $\beta$ -FeOOH) might grow in marine environments (Selwyn et al. 1999; Réguer et al. 2007; Rémazeilles and Refait 2007). Growth of akaganeite requires high concentrations of both Fe(II) and chloride ions (Rémazeilles and Refait 2007). Due to the shielding effect of the magnetite layer, high concentrations of both kinds of ions can be reached at the magnetite-metal interface. Rémazeilles and Refait (2007) also showed that the growth rate of akaganeite but not growth per se depends on the DMO concentration in the electrolyte. Akaganeite crystals always grow from the metal surface towards the magnetite layer and their volume is significantly larger than that of the metallic iron. As a consequence, they will build up pressure on the magnetite layer and overlying corrosion products to an extent that it will crack and even spall (Selwyn et al. 1999).

In non-permanently water-logged environments, usually high levels of DMO prevail and goethite is formed as a corrosion product. In contrast to magnetite, goethite is non-conductive but porous and DMO can easily diffuse through it until the pores are cemented with goethite. As soon as the corrosion layer dries, the dissolved iron compounds in the electrolyte start to crystallise, especially the iron chlorides (Réguer et al. 2006, 2007). Due to their bigger volume, cracks will evolve in the corrosion layer. Molecular oxygen can now diffuse again into the corrosion layers and to the metal surface. It will rapidly oxidise any aqueous ferrous to ferric hydroxide, which will precipitate and convert to goethite. This reaction lowers the pH of the remaining solution and thus promotes further corrosion of the iron object even after all aqueous Fe(II) has been oxidised (Selwyn et al. 1999).

The resulting corrosion layers can be subdivided into four different sub-layers according to the model proposed by Neff et al. (2004, 2005) for terrestrially buried iron objects: The innermost layer is the metallic substrate, which represents the uncorroded material. This is covered by the “dense product layer” (DPL). The DPL consists of corrosion products like Fe (hydr)oxides, carbonates, or chlorides. This zone may contain internal markers of the metal, such as slag inclusions. The composition of the DPL depends on the environment. In oxidised environments, it consists of goethite with veins of magnetite or maghemite. Cracks are often filled with Fe phosphates or carbonates and mostly occur parallel to the original surface of the object. The DPL in water-logged environments is characterised by a thick siderite and a thin magnetite layer (Matthiesen et al. 2013; Michelin et al. 2013). Due to the well-crystallised corrosion products, the DPL is more compact than the subsequent zone. This next layer, called “transformed

medium" (TM), is the transition zone between DPL and the soil. It consists of Fe (hydr)oxides, which were dissolved in the DPL by soil water and precipitated here due to the more oxidising conditions. Thus, its crystallinity is rather low and the sublayer is a mixture of corrosion products and soil markers, such as quartz grains. The interface between the DPL and the TM is regarded as the original surface of the metal, but its actual position can shift during corrosion (Neff et al. 2005). The outermost zone is soil, unaffected by the corrosion process (Neff et al. 2004, 2005).

### Potential of isotope fractionation during corrosion

Iron isotopes were recently proposed as a new tool in archaeometallurgy (Milot 2016; Milot et al. 2016). The determination of O isotope compositions of artefacts seems promising as they are widely used as climate proxy and the corrosion layer might record climatic information similar to bog iron ores (Yapp 1987; Poage et al. 2000; Sjöström et al. 2004).

### Iron isotopes

So far, studies about the behaviour of Fe isotopes during corrosion of iron artefacts are lacking. But consideration of similar processes like Fe dissolution during weathering of Fe minerals and precipitation of Fe (hydr)oxides in bog iron ores allow a first estimate. According to a thermodynamic model of the corrosion process developed by Neff et al. (2006), Fe will not be significantly lost during long-term corrosion under oxidising conditions. This might be different during the initial phase of the corrosion process.

Iron isotope fractionation in soils is governed by a complex mixture of processes, most notably complexation with organic compounds and the uptake of complexed iron by plants (Fantle and DePaolo 2004; Wiederhold et al. 2007), loss of dissolved Fe into deeper soil horizons or laterally (Wiederhold et al. 2007), and changes in the redox environment (Schuth et al. 2015). Under reducing conditions, Fe isotope fractionation during dissolution of Fe in soils rich in ferrihydrite and organic material is strongly affected by changes in the redox environment, while it does not seem to have a significant impact on Fe isotope fractionation in goethite rich soils (Schuth et al. 2015), most likely because of the much smaller mobility of Fe(III) compared with that of Fe(II). The latter observation corresponds well with the overall higher solubility of Fe during the corrosion of iron objects in reducing soil environments (Neff et al. 2006).

Although it is very difficult to rule out the impact of each single process on the observed Fe isotope fractionation in natural systems, there are indications that the dissolution of Fe (Eq. 1) might not fractionate Fe isotopes. Li et al. (2017) report a very limited fractionation of Fe isotopes for the dissolution of Fe during laterite formation. Their data shows a

shift towards heavier isotope compositions in the remaining material but a certain influence by loss of isotopically light Fe to organic complexes cannot be ruled out. Yesavage et al. (2012) suggested two models for the dissolution, transport, and precipitation of Fe during the weathering of shale on a hill slope, with fractionation of Fe isotopes during dissolution or precipitation, respectively. The best agreement with their data was achieved when Fe isotopes did not fractionate during the dissolution. Hence, it might well be that the dissolution of Fe does not fractionate Fe isotopes but that the dissolved Fe immediately interacts with the soil components and its isotopes get fractionated.

Immediate interaction of the object or iron dissolved from it with the soil might be important during the initial stages of the corrosion process. However, as soon as the dissolution of Fe from the object is separated from the soil environment by an insoluble layer of corrosion products, Fe isotope fractionation during dissolution of Fe from the metal should only be influenced by the dissolution reaction itself and thus is probably negligible. Consequently, the Fe isotopic composition of an artefact might not be affected by alteration in the long term. During the initial stages of the corrosion process, only the surface of the iron object might have a Fe isotope composition different to the bulk metal.

Precipitation of Fe (hydr)oxides and formation of goethite from Fe(III) might fractionate Fe isotopes, as the lighter isotopes are enriched in the goethite (Skulan et al. 2002; Wiederhold et al. 2007; Kiczka et al. 2011). However, a constant exchange between small crystals of goethite (< 500 nm) and dissolved Fe develops by the dissolution of preferentially lighter Fe isotopes from goethite (Jang et al. 2008; Poulson et al. 2005) and absorption of reduced Fe(II) (Hansel et al. 2005), balancing the isotopic composition of both over time (Handler et al. 2009; Reddy et al. 2015; Wu et al. 2011). This effect was questioned for larger crystals, which might preserve their initial isotopic composition (Handler et al. 2014). If there is no Fe isotope fractionation during dissolution of Fe and the dissolved Fe quantitatively reacts to goethite, the Fe isotope composition of the corrosion products becomes identical to the dissolved iron's one, which again is identical with the Fe isotope concentration of the metal. For purely goethite-containing corrosion products, this would result in identical Fe isotope compositions of the already present corrosion products and the new corrosion products precipitated in their cracks and pores, i.e. isotopic homogeneity within the corrosion layer. Only in a subsequent stage the remaining dissolved Fe will be transported to the outer surface of the corrosion products (Neff et al. 2005, 2006). Here, it most likely will become isotopically fractionated during the interaction with the soil (Fantle and DePaolo 2004; Schuth et al. 2015; Wiederhold et al. 2007) or because the concentration of dissolved Fe in the pore fluid of the soil is too unstable to achieve the above-mentioned balance between dissolved Fe and goethite.

Little is known about the precipitation of magnetite. If it is precipitated in a Fe(II) ion-bearing solution from ferrihydrite, magnetite becomes enriched in the heavier isotopes compared with aqueous Fe(II), and isotopic equilibrium is nearly reached within 14 days (Friedrich et al. 2014b). Isotopic equilibrium between magnetite and aqueous Fe(II) is reached after about 10 days and magnetite becomes enriched in the heavier isotopes compared to aqueous Fe(II) (Gorski et al. 2012; Friedrich et al. 2014b). The fractionation factor of this reaction seems to be strongly influenced by the stoichiometry of the magnetite (Friedrich et al. 2014b).

There are no studies published to date on the Fe isotope fractionation involving akaganeite.

## Oxygen isotopes

Oxygen in the corrosion products has two different origins (see Eqs. 2 and 3): DMO and water. Atmospheric oxygen represents a source for DMO. Molecular oxygen in the air has  $\delta^{18}O_{\text{Air-O}_2} = +23.88\text{‰}$  relative to V-SMOW (Brand et al. 2014). The O isotope composition of DMO is enriched in the heavier isotope by around 0.7‰ in equilibrium with atmospheric oxygen (Benson and Krause 1984; Knox et al. 1992; Hendricks et al. 2005; Li et al. 2019). This would result in  $\delta^{18}O_{\text{DMO}} \sim +24.6\text{‰}$  and hence an enrichment of the heavier O isotope in DMO by 24.6‰ compared with seawater. The salinity of the water has no effect on this fractionation (Kroopnick and Craig 1972; Benson and Krause 1984). Besides dissolution from atmospheric molecular oxygen, DMO can also be the product of photosynthesis from water molecules within the water body. Photosynthesis or, more precisely, photolysis does not fractionate O isotopes, generating DMO with the same O isotopic composition like the water body (Benson and Krause 1984; Guy et al. 1993). DMO originating from both sources is mixed, and the resulting O isotope composition depends on the contributions from both origins. At the same time, respiration consumes DMO. Organisms preferentially take up the lighter isotopes, leading to a heavier isotopic composition in the remaining DMO. Inorganic respiration has the same effect but fractionates O isotopes to a much smaller extent (Aggarwal and Dillon 1998; Angert et al. 2001). With depth, the contribution by respiration becomes more important, leading to an overall heavier O isotope composition of DMO with increasing depth in seawater (Hendricks et al. 2005).

Moreover, the isotopic composition of DMO in groundwater and soils is affected by additional parameters. For oxygen to dissolve in groundwater, it has to diffuse from the atmosphere into the soil gas first. Due to its lighter mass,  $^{16}\text{O}$  diffuses significantly faster than  $^{18}\text{O}$  and the O isotope composition of the soil gas becomes lighter up to 14‰, increasing with increasing depth (Aggarwal and Dillon 1998). A high

porosity and big pores enhance the diffusivity of oxygen, shifting the O isotopic composition towards lighter values. Evaporation of the pore water after irrigation also enhances the diffusion of oxygen in the soil, leading to a rising oxygen concentration and lighter O isotopic composition the more time passed since the last irrigation (Angert et al. 2001). As a result, the isotopic composition of the DMO finally reaching the metal object and being used in Eq. 2 can hardly be reconstructed but should be measured directly.

According to Eq. 2, the O isotope compositions of water and DMO contribute equally to the O isotope composition of the hydroxide ions.

The hydroxide ions will then combine with aqueous Fe(II) (Eq. 3). Unfortunately, no experiments starting from metallic iron are reported in the literature yet for this reaction. Experimental oxidation of aqueous Fe(II) deriving from ferrous sulphate by DMO revealed an enrichment of the lighter isotope in the ferrous hydroxides by 7.3 to 10.3‰ in neutral and 4.5 to 11.6‰ in acidic solutions (Oba and Poulson 2009). Although the results of these experiments cannot be directly transferred to most of the corrosion environments, the observed enrichment of the lighter isotopes in the Fe(II) ions will presumably also occur here.

As was shown above, the further development of the corrosion products depends on the pH and the concentration of DMO. First, all or only a part of the ferrous hydroxides will be oxidised to ferric hydroxide by incorporating another hydroxide ion derived from Eq. 1. Subsequently, part of the oxygen will be released as water during the crystallisation of magnetite, akaganeite, and goethite. However, experiments targeting isotopic fractionation associated with these processes were not reported yet.

However, all these reactions take place in water as a medium. Should oxygen isotope equilibrium between water and the reaction product finally be attained, the oxygen isotopic composition of the water could finally be reconstructed if the alteration temperature and the temperature dependence of the equilibrium oxygen isotope fractionation between water and the reaction product were known.

Temperature curves for the O isotope fractionation between magnetite and water have so far only been established for the high-temperature ranges. All of these suggest an enrichment of  $^{16}\text{O}$  in magnetite but they scatter over nearly 12‰ at 25 °C (Yapp 1990; Mandernack et al. 1999).

Oxygen isotope fractionation factors between akaganeite and water were reported by two studies. The heavier isotopes seem to be enriched in the akaganeite but their values differ by more than 4‰ at 25 °C, with the smaller fractionation reported as 1.0‰ (Bao and Koch 1999) and the larger one as ~5.5‰ (Xu et al. 2002). Furthermore, Bao and Koch (1999) state that evaporation of the remaining water during sample preparation

seems to have a significant effect on the measured O isotope fractionation factors.

Several studies investigated the O isotope fractionation between water and goethite during the precipitation of goethite (e.g. Bao and Koch 1999; Yapp 1990; Friedrich et al. 2015), mostly with the aim to reconstruct palaeotemperatures (e.g. Sjostrom et al. 2004; Yapp 1987, 2008). In all the synthesis experiments, goethite was directly precipitated from Fe(III) ions due to the much faster reaction compared with natural processes. Most experiments were conducted at pH 2 or 14 (Yapp 2001). Both circumstances limit their applicability to the corrosion process. Moreover, fractionation factors reported in the literature scatter over 8‰ at 25°C (Friedrich et al. 2015).

Analysis of goethite in bog ores and their associated groundwaters revealed a small or even negligible enrichment of the heavier isotope in the goethite (Bao and Koch 1999; Friedrich et al. 2015). Isotopic equilibrium is rapidly approached (Friedrich et al. 2015) and fully crystallised goethite does not exchange O isotopes with the solution (Bao and Koch 1999). Consequently, goethite might reflect the O isotope composition of its source water.

With respect to bog iron ores, Bao et al. (2000) came to the conclusion that not the groundwater should be analysed but the soil water from which they precipitated. This necessitates to consider evaporation. Evaporation experiments show that after evaporation of 75% of the initial amount of water at 10 °C, the remaining water was enriched in <sup>18</sup>O by 37.58‰ (Luz et al. 2009). Unfortunately, the soil water is difficult to reconstruct, rendering palaeotemperature reconstructions nearly impossible (Bao et al. 2000; Yapp 2008). Further parameters like particle size (Friedrich et al. 2015), pH and chloride (e.g. Yapp 2007), and Al concentration (e.g. Yapp 2012) in goethite will also have some influence on the extent of the fractionation. But they will not be taken into account in this study, because suitable data are lacking for the sample material and because they seem to have only a minor effect with regard to the strong fractionation expected through evaporation (Bao et al. 2000).

The O isotope fractionation between haematite and water is nearly identical to that for goethite–water. The observed enrichment of the heavier isotope in the haematite during its formation from goethite can be explained by evaporation (Bao et al. 2000; Blanchard et al. 2015).

## Aim of the study

This study investigates for the first time the stable Fe and O isotope composition of iron corrosion products on iron artefacts. The aim is to investigate to what extent fractionation of Fe and O isotopes occur during corrosion. Analysed specimens were collected from marine environments and water under-saturated oxidising environments. Based on the results, an attempt is made to identify potential trends and suggest possible applications of Fe isotope analysis and O isotope

analysis of Fe corrosion layers. Due to the small sample size, results from this study can only be regarded as preliminary and hopefully stimulate further research.

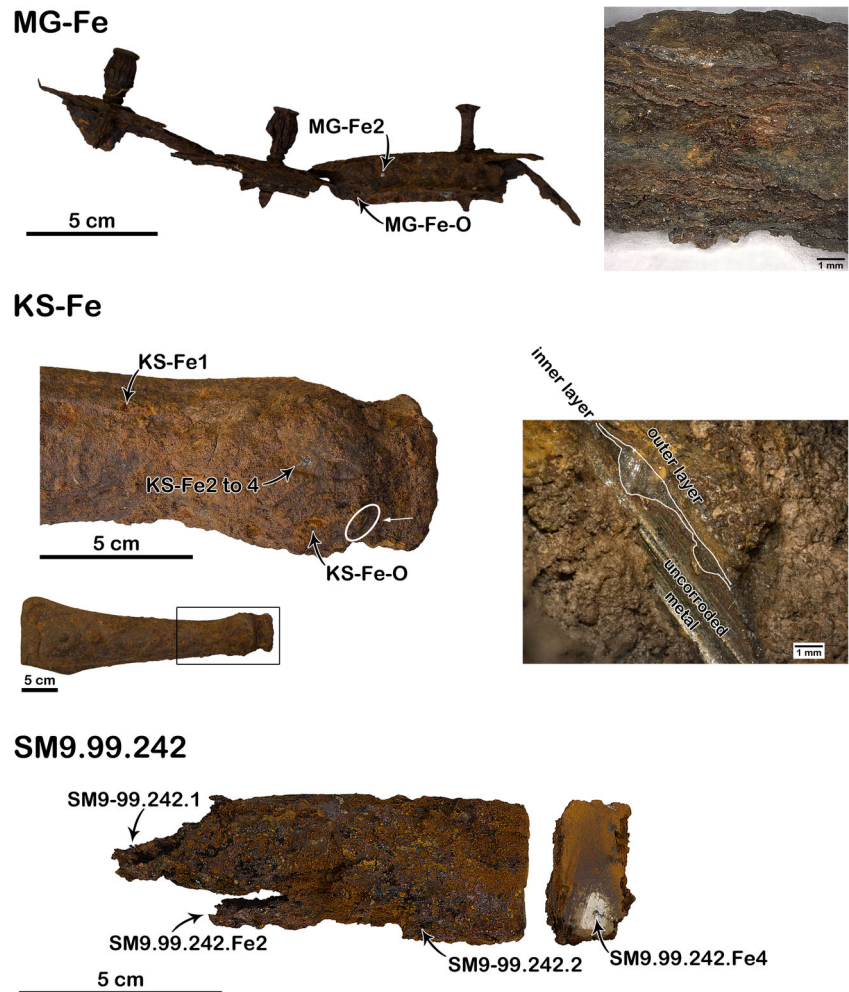
## Sample material

Four different Fe-bearing items were investigated for this study (Fig. 1 and 2). The steel profile MG-Fe (Fig. 1) was originally installed in the lower part of an open composter in Munich, Germany (Fig. 3), around 20 years ago. The outside was partly exposed to the atmosphere and partly covered by wooden laths while the inner surface was in contact with humus and decaying organic material. It is heavily corroded and almost no metallic core is preserved. The dark red–blackish corrosion products formed platelets with varying thickness parallel to the original surface. XRD analysis and subsequent Rietveld refinement with GSAS II (Toby and von Dreele 2013) gave a mineralogical composition of ~30% goethite and 70% magnetite or maghemite (diffraction patterns of both were indistinguishable). Samples along two profiles were taken for iron isotope analysis: one set of samples along a profile from the surface in contact with the compost towards the core (MG-Fe-1.1 to 1.5) and another from the surface in contact with the atmosphere to the core (MG-Fe-2.1 to 2.3). In the latter profile, the metallic core is well preserved (MG-Fe-2.3). For O isotope analysis, a profile from the metallic core (MG-Fe-O2) to the interior surface (MG-Fe-O5) was sampled. MG-Fe was generously provided by M. Giroto.

The object KS-Fe (Fig. 1) was found in 2009 in the vicinity of the Klause near Kastel-Staadt, Germany. It was located in the poorly plant-covered sandy topsoil of the slope of the Saar valley (Fig. 3a) at ~10 cm depth. Based on the shape and preserved ornamentation, it was the leg of an Art Nouveau cast-iron stove, dating between 1880 and 1910. The corrosion products consist of an outer porous orange-brown layer and an inner dark red-greyish layer with an overall thickness of ~2 mm. The interface between both layers seems to indicate the original surface of the object. Additionally, blistered areas of corrosion products are scattered over the surface. Material sampled by XRD consists of goethite and mostly soil (~80% quartz and feldspar). For iron isotope analysis, all of these products and the metallic core were sampled. KS-Fe1 represents material from a blistered structure, whereas KS-Fe2 contains material from the outer and KS-Fe3 from the inner corrosion layer. KS-Fe4 was taken from the metallic core. For O isotope analysis, samples were taken from the outer (KS-Fe-O1) and the inner corrosion layer (KS-Fe-O2), respectively.

The semi-product SM9.99.242 (Fig. 1) is part of the cargo from the Roman ship SM9, which sunk in the Gulf of Lion near Les-Saintes-Maries-de-la-Mer (Bouches-du-Rhône, France; Fig. 3c) and dates between 14 and 50 CE (Long et al. 2002; Pagès 2008; Pagès et al. 2008). The specimen

**Fig. 1** Photographs of the objects with the location of the sampling spots. For MG-Fe and KS-Fe additional microphotographs are shown. For MG-Fe, it shows the layered structure of the corrosion product in a detached fragment. The microphotograph from KS-Fe was taken from a cut. Its position and the direction of view are indicated by the white ellipsis and the arrow



was recovered from a depth of 12 to 13 m (Long et al. 2002). It belongs to the type 1C, is more than half a metre long with a rectangular cross-section of 4.0 cm × 1.9 cm, and weighs about 2.4 kg (Long, pers. comm., 2018). It was graciously provided by L. Long (Marseille) and is an example of marine corrosion. Two types of corrosion products were identified: comparatively hard and dark-grey rust, which is firmly connected to the metallic core and partially covered with dark-orange crumbly material, and detached small bright orange particles. The dark-grey rust with the crumbly particles consists entirely of akaganeite according to XRD analysis. Samples for iron isotope analysis were taken from a detached particle of black rust (SM9.99.242.Fe1), black rust connected to the semi-product (SM9.99.242.Fe2), the loose orange material (SM9.99.242.Fe3), and the metallic iron (SM9.99.242.Fe4). For O isotope analysis, black rust from two different spots was analysed.

The iron ore specimen of the Lahn-Dill type ore-W (Fig. 2) was collected from an ore heap in a forest about 5 km south-west of Wetzlar, Germany (Fig. 3b), an area extensively mined for iron ore from the eighteenth century until the

twentieth century. It consists mostly of haematite and is intensively crossed by quartz veins. Its exposed surface indicates prolonged weathering due to the typical orange-brown colour of iron (hydr)oxides. Initially part of another study (ore-W1 to 4) (Rose et al. 2019), this surface was additionally sampled for iron isotope analysis (ore-W5 & 6) as a comparison for the weathering of exposed surfaces.

## Methods

### Fe isotope analysis

#### Sample preparation

The use of steel tools was reduced to a minimum to avoid contamination. Most of the samples were drilled from each specimen with diamond-sputtered steel drills of 1.2 mm in diameter and a Dremel 4000. The drills were cautiously examined under a stereomicroscope after cleaning for remnants of sample material or any damages to the drill. Differing from



**Fig. 2** Photograph of the hydrothermally altered haematite ore specimen ore-W with the location of the different sampling spots

this, the Profile MG-Fe-1 was sampled by detaching small areas of already partially loosened lamellae with a lancet.

Analytical work was carried out in a clean lab under a laminar flow box at the Institut für Geowissenschaften, Goethe Universität Frankfurt. Millipore® water with a resistivity of 18.2 MΩ·cm, double-distilled acids, and PTFE beakers were used throughout the analytical process. The amount of each sample used for the analysis is given in Table 1. All samples except the ore samples were completely dissolved in 1 ml of each, 6 M HCl and 6 M HNO<sub>3</sub>, heated on a hot plate to 90°C until complete dissolution was achieved (several hours). The ore samples were dissolved in ~2 ml 30 M HF + 6 M

HNO<sub>3</sub> and heated to the same temperature overnight. All samples were dried down at 90°C, re-dissolved in 1 ml 6 M HCl, and dried down again before they were taken up in 0.5 ml 6 M HCl for ion-exchange chromatography.

The ion-exchange chromatography protocol of Sossi et al. (2015) for columns of 70 mm length and an inner diameter of 4 mm was adapted for the resin AG1-X8 (100 to 200 mesh). Several samples were split prior to ion-exchange chromatography to check for ion-exchange chromatography induced Fe isotope fractionation, which was demonstrated to be absent. Samples were dried down at ~70°C after ion exchange chromatography, re-dissolved in 1 ml 6 M HNO<sub>3</sub>, and evaporated to dryness to remove remnants of the resin.

**Mass spectrometry**

Iron isotope analysis was carried out with the multi-collector plasma mass spectrometer ThermoFisher NeptunePlus of the Laboratoire de Géologie de Lyon, École Normale Supérieure de Lyon. It was operated in a high-resolution mode (Weyer and Schwieters 2003) and equipped with Ni cones, a quartz glass cyclonic spray chamber and a Glass Expansion MicroMist nebuliser. Samples were dissolved on site in 2% HNO<sub>3</sub> and further diluted with 0.05 N HNO<sub>3</sub>. Mass bias and instrumental drift were corrected by doping with 1 µg/g Ni (Maréchal et al. 1999; Poitrasson et al. 2005) prepared from the Alfa-Aesar Specpure® Ni plasma standard solution and standard-sample-bracketing with the international reference

**Fig. 3** Location of the collected specimens and the position of the Roman shipwreck SM2 (maps: [openstreetmap.org](http://openstreetmap.org))

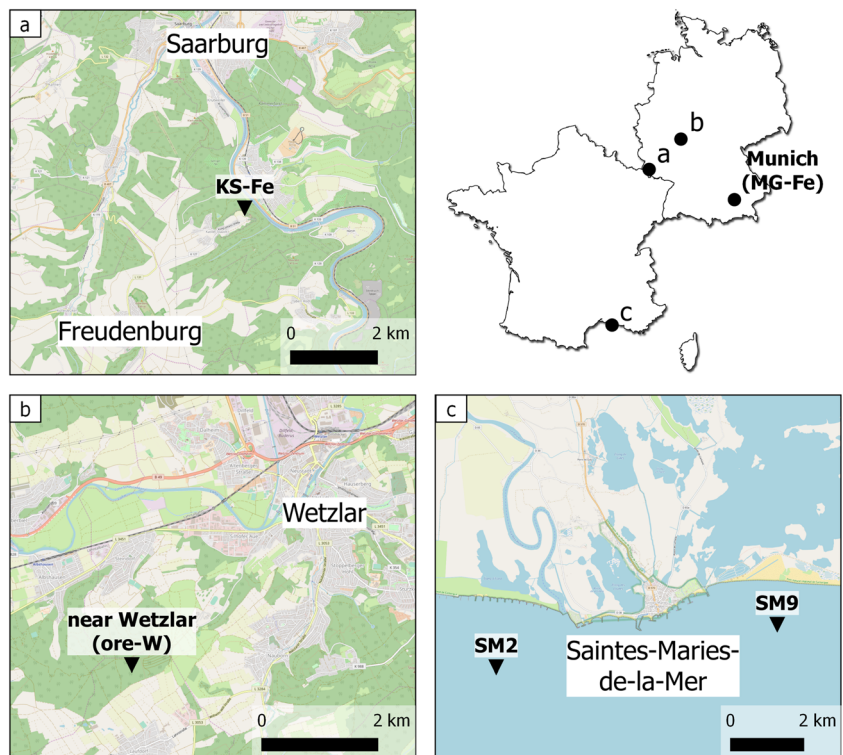


**Table 1** Mass and Fe isotope compositions of the analysed samples. Analytical precision for all samples is 0.09‰ for  $\delta^{56}\text{Fe}$  and 0.14‰ for  $\delta^{57}\text{Fe}$ . The last column gives the number of analyses (n) per sample

Sample	Mass [mg]	$\delta^{56}\text{Fe}$ [‰]	$\delta^{57}\text{Fe}$ [‰]	n
Kastel-Stadt, oven leg				
KS-Fe1	11.4	0.04	0.03	4
KS-Fe2	1.4	0.26	0.40	4
KS-Fe3	4.6	-0.03	0.02	1
KS-Fe4	0.6	-0.04	-0.02	2
Munich, steel profile				
MG-Fe-1.1	1.3	0.18	0.26	2
MG-Fe-1.2	2.4	0.28	0.37	2
MG-Fe-1.3	1.4	0.27	0.39	1
MG-Fe-1.4	3.0	0.21	0.30	2
MG-Fe-1.5	1.4	0.19	0.36	2
MG-Fe-2.1	1.3	0.20	0.31	2
MG-Fe-2.2	1.9	0.19	0.34	1
MG-Fe-2.3	0.8	0.18	0.24	1
Les Saintes-Maries-de-la-Mer, Roman semi product				
SM9.99.242.Fe1	10.5	-0.35	-0.49	4
SM9.99.242.Fe2	3.9	-0.47	-0.73	2
SM9.99.242.Fe3	3.3	-0.30	-0.47	2
SM9.99.242.Fe4	2.8	-0.31	-0.48	2
Near Wetzlar, haematite ore				
Ore-W1 (Rose et al. 2019)	1.3	0.76	1.12	2
Ore-W2 (Rose et al. 2019)	1.4	1.00	1.48	1
Ore-W3 (Rose et al. 2019)	2.7	0.69	1.03	1
Ore-W4 (Rose et al. 2019)	0.9	0.49	0.71	2
Ore-W5	2.7	0.03	0.02	5
Ore-W6	6.8	-0.10	-0.11	4

material IRMM-014 (Taylor et al. 1992; Craddock and Dauphas 2011). Samples and standards were taken up for 50 s. Blanks were measured before each analysis. A total of 1  $\mu\text{g/g}$  of IRMM-014 yielded an intensity of  $\sim 10$  V on  $^{56}\text{Fe}$ .

$\delta^{56}\text{Fe}$  values were calculated in a spreadsheet after online mass bias correction according to the equation:

$$\delta^{56}\text{Fe} [\text{‰}] = \left[ \frac{\left( \frac{^{56}\text{Fe}}{^{54}\text{Fe}} \right)_{\text{smp}}}{\left( \frac{^{56}\text{Fe}}{^{54}\text{Fe}} \right)_{\text{IRMM-014}}} - 1 \right] \cdot 1000$$

Here, the index *smp* denotes the ratio  $^{56}\text{Fe}/^{54}\text{Fe}$  of the sample and the index IRMM-014 denotes the ratio of the international reference material. The  $\delta^{57}\text{Fe}$  values are calculated accordingly.

Each sample was run twice as duplicates and some samples were repeatedly measured in different sessions to check for inter-run stability. Data were further processed with R (R Core Team 2017) in RStudio®. If amu-

normalised  $\delta$  values within one measurement differed by more than the instrumental reproducibility of 0.045‰/u, this measurement was identified as an outlier and not regarded further. All other values were averaged and resulted in the reported values. Procedural blanks yielded intensities more than 10,000 times lower than sample intensities. The external reproducibility ( $2\sigma$ ) of the analyses is  $< 0.05\text{‰/u}$ , which is comparable with that of previous studies (Albarède et al. 2011; Balter et al. 2013).

## Oxygen isotope analysis

Samples were extracted with a lancet or tweezers and placed in a vacuum drying oven at 100°C and 2.5 kPa overnight to evaporate free water in the sample. Before sampling, all specimens were cautiously examined under a stereomicroscope to exclude the presence of organic material. Despite its big tunnels, akaganeite does not incorporate water in the crystal lattice (Ståhl et al. 2003).

The O isotope analysis was carried out at the Joint Stable Isotope Lab of Goethe University Frankfurt and the Senckenberg Biodiversity and Climate Research Centre BiK-F. The amount of each sample used for the analysis is given in Table 2. Oxide oxygen was quantitatively extracted as molecular oxygen using  $\text{CO}_2$  laser fluorination and purified fluorine as a reagent. Isotopic compositions were determined with a ThermoFinnigan MAT253. An in-house quartz standard (L1,  $\delta^{18}\text{O} = -18.2\text{‰}$ ) and UWG 2 ( $\delta^{18}\text{O} = -5.9\text{‰}$ ) (Valley et al. 1995) were analysed along with the samples to monitor the accuracy and precision of oxygen extraction.  $\delta^{18}\text{O}$  values are reported relative to the international standard V-SMOW (IAEA 2017). External reproducibility is  $< 0.2\text{‰}$  ( $1\sigma$ ).

**Table 2** Mass and O isotope compositions of the analysed samples. Analytical precision for all samples is 0.02‰

Sample	Mass [mg]	$\delta^{18}\text{O}$ [‰]
Kastel-Stadt, oven leg		
KS-Fe-O1	2.222	8.5
KS-Fe-O2	2.409	9.5
Munich, steel profile		
MG-Fe-O2	1.911	-2.0
MG-Fe-O3	1.966	-2.0
MG-Fe-O4	1.613	-2.6
MG-Fe-O5	1.820	-1.7
Les Saintes-Maries-de-la-Mer, Roman semi product		
SM9-99.242.1	1.858	1.1
SM9-99.242.2	1.814	1.3

## Results

Iron isotope compositions for all samples are given in Table 1. In all three iron objects, samples were isotopically indistinguishable (Fig. 4). For KS-Fe, three of four analyses show  $\delta^{56}\text{Fe}$  values close to 0.00‰. Only KS-Fe2 yielded a value of  $\delta^{56}\text{Fe} = +0.26\text{‰}$  and thus is isotopically significantly heavier than the other samples. Isotopic compositions for MG-Fe vary between +0.18 and +0.28‰. In the Roman semi-product SM9.99.242, only the sample SM9.99.242.Fe2 displays a slight apparent enrichment of the lighter isotopes, but within analytical precision. All other samples possess  $\delta^{56}\text{Fe}$  values close to +0.32‰.

In the ore specimen, a considerable enrichment of the lighter isotopes on the surface (Ore-W5 and 6) compared with the interior was observed ( $\delta^{56}\text{Fe}_{\text{surface-interior}} = -0.76\text{‰}$ ). The isotopic composition of the interior is quite heterogeneous (Fig. 4).

Oxygen isotope data are given in Table 2 and are plotted in Fig. 5. The two samples from the Roman semi-product SM9.99.242 yielded an identical isotopic composition of  $\delta^{18}\text{O} \sim +1.2\text{‰}$ . In MG-Fe, one sample shows with a  $\delta^{18}\text{O}$  value of  $-2.6\text{‰}$  an enrichment of the lighter isotopes compared with the other samples, which vary between  $-2.0$  and  $-1.7\text{‰}$ . The outer corrosion layer of KS-Fe yielded an O isotope composition of  $\delta^{18}\text{O} = +8.5\text{‰}$ , while the inner corrosion layer yielded  $\delta^{18}\text{O} = +9.5\text{‰}$ .

## Discussion

### Marine corrosion

#### Iron isotopes

Samples from SM9.99.242 yielded indistinguishable Fe isotope values. Milot et al. (2016) reports a sample of marine corrosion from the same shipwreck, which has a lighter isotopic composition than the uncorroded metal (SM9-99-K46). His two isotope dates for the metal as well as the isotopic composition of the marine corrosion lies within the spread of the data derived from SM9.99.242. The analytical precision of the  $\delta^{56}\text{Fe}$  value and of

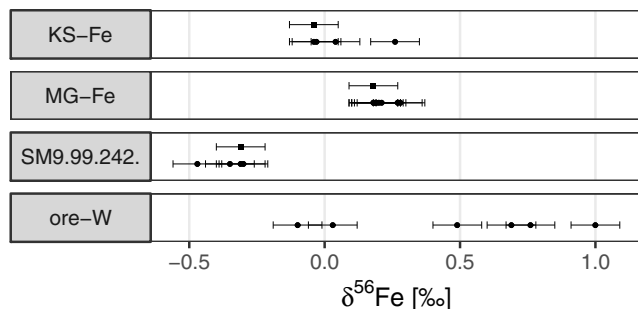


Fig. 4 Fe isotope compositions of the analysed objects. The squares denote the Fe isotope composition of the metallic cores

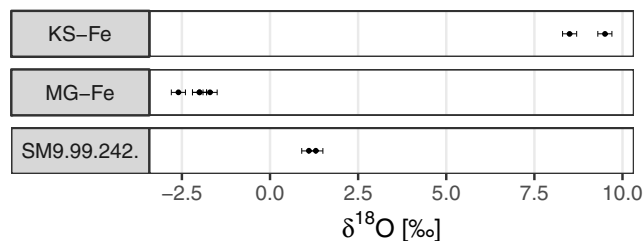


Fig. 5 Oxygen isotope data of the analysed objects

the  $\delta^{57}\text{Fe}$  value shows a considerably higher variation than the other data of his data set resulting in overlapping data of metal and marine corrosion products within their standard errors for  $\delta^{56}\text{Fe}$  but not for  $\delta^{57}\text{Fe}$  (Milot 2016, p. 208). For a semi-product from a different shipwreck (SM2) located nearby (Fig. 3c), he reports an isotopically slightly heavier composition of the corrosion layer compared with the metallic core, which is the opposite trend compared with SM9-99-K46. Unfortunately, Milot et al. (2016) does not report any information about the phase composition of the corrosion products.

Marine corrosion under stable conditions results in a protective layer of magnetite, which strongly decelerates corrosion (Memet 2007). Once the protective layer was formed, an exchange between the electrolyte and the ocean water is strongly reduced and prevents Fe ions from being washed out.

Fe isotope fractionation between water and akaganeite during the growth of akaganeite was not investigated so far. Although Fe isotope fractionation must be expected to some extent as it has the same chemical composition as goethite and they share some similarities in their crystal structures, indistinguishable Fe isotope data of the corrosion layer and the metal shows the absence of fractionation between the two. This can only be achieved by the precipitation of all aqueous Fe(II) in the corrosion products, i.e. negligible loss of aqueous Fe(II) into the seawater. Such a negligible loss was proven for terrestrial corrosion (Neff et al. 2006) and the shielding effect by the initial magnetite layer gives no reason to assume a different situation in marine corrosion.

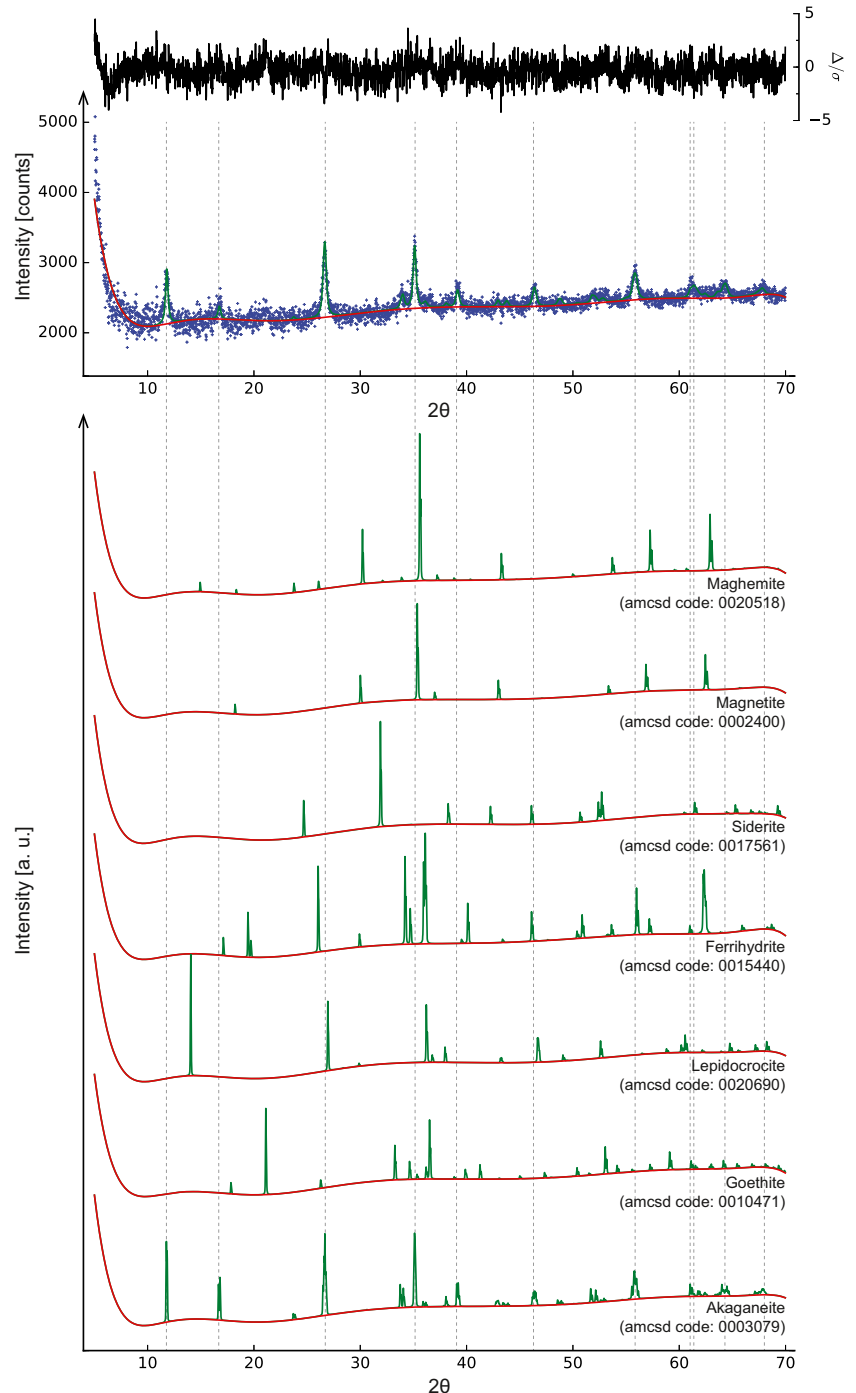
A possible explanation for such a quantitative precipitation of aqueous Fe(II) in the electrolyte is the removal of chloride ions out of the electrolyte as one of the major strategies in iron conservation. To reach this aim, the objects are stored for a prolonged time in a solution, which is regularly changed (North and Pearson 1978; Rimmer et al. 2013; Selwyn and Argyropoulos 2013). Among them, a deoxygenated NaOH solution seems to be the most efficient (Rimmer et al. 2013; Selwyn and Argyropoulos 2013). This treatment removes not only the chloride but also rises the pH of the electrolyte, allowing quantitative precipitation of the aqueous Fe(II) in the pore space of the corrosion products. There are indications for terrestrial oxidising conditions that dissolution of Fe does not fractionate Fe isotopes (Li et al. 2017; Yesavage et al. 2012). It must remain unclear if this holds true for metallic

iron and marine conditions, but if it does, the dissolved Fe has the same isotopic composition as the metal. As a consequence, quantitative precipitation of the dissolved Fe results in corrosion products with the same isotopic bulk composition as the original metal. Within the corrosion layer, differences in the isotopic composition between the precipitate and the corrosion products cannot be excluded. The treatment does not affect the akaganéite and the chloride ions stabilising its crystal structure (Stähl et al. 2003). However, the decreased

concentration of free chloride ions will prevent the formation of new akaganéite and the Fe ions will precipitates as other phases. But this seems not to be the case, as XRD analyses gave no indication for the presence of another phase (Fig. 6), rendering the desalination treatment as a reason for uniform Fe isotopic compositions unlikely.

It seems more convincing that the aqueous Fe(II) quantitatively precipitated before the semi-product was recovered from the shipwreck. Like in the first scenario, the shielding

**Fig. 6** Diffraction pattern of SM9.99.242 compared with various iron corrosion phases. The observed data are represented as blue +, the calculated pattern of each phase as a continuous green line, and the background fit as a red line. On top of the refined diagram, the plot (observed – calculated difference)/(estimated standard deviation) ( $\Delta/\sigma$ ) for akaganéite is shown. Phases for comparison were downloaded from the American Mineralogist Crystal Structure Database (Downs and Hall-Wallace 2003) and calculated without any refinement on the background fit of the refined diagram



effect of the magnetite layer causes concentrations of chloride and Fe(II) ions in the electrolyte high enough to allow the growth of akaganeite and negligible Fe isotope fractionation occurs during the dissolution of the metallic iron. Over time, akaganeite crystals filled the entire space between the metal surface and the magnetite layer, leaving only minor amounts of the electrolyte behind. The compactness of the layer might indicate low levels of DMO and a slow, well-ordered crystallisation. This slow crystallisation might have been enhanced by a strongly slowed down exchange between aqueous Fe(II) and Fe(III) due to the high chloride content (Welch et al. 2003). The strong Fe isotope fractionation reported by Welch et al. (2003) for this exchange reaction ( $\Delta^{56}\text{Fe}_{\text{Fe(II)-Fe(III)}} \sim 2.8\text{‰}$  at 22°C) might have been balanced by a similar exchange mechanism between akaganeite and dissolved Fe as it was identified for goethite, where it leads to an identical Fe isotope composition of goethite and dissolved Fe (Friedrich et al. 2015; Jang et al. 2008; Reddy et al. 2015). Because small amounts of the electrolyte are sufficient to keep the corrosion reaction proceeding, growth of akaganeite continued and finally resulted in the spalling of the overlying corrosion products (cf. Selwyn et al. 1999). In this scenario, the amount of precipitated iron phases from desalination would have been at least negligible with respect to XRD analysis, leading to the observation of a mono-phase corrosion layer with the same Fe isotope composition as the metal. Likewise to the interactions in the soil, the Fe isotope composition of the corrosion layer's outer surface might be altered due to dissolution and isotope exchange processes between corrosion and seawater.

Nevertheless, this model fails to explain the slight enrichment of the heavier Fe isotopes in the corrosion layer of the semi-product from shipwreck SM2 compared with its metal, which is reported by Milot et al. (2016). The observed fractionation would be in accordance with the results of equilibration experiments with magnetite in aqueous Fe(II)-containing solution (Gorski et al. 2012; Friedrich et al. 2014b). Unfortunately, the mineralogical composition of the corrosion products was not reported. In addition, the shipwreck is located nearly 11 km west of SM9 (Fig. 3c), which might be sufficient to establish different local conditions. Hence, this observation cannot be further discussed.

Similarly, the corrosion data from semi-product SM9-99-K46 reported by Milot et al. (2016) cannot be further discussed because no information about the mineralogical composition is given and its  $\delta^{56}\text{Fe}$  and  $\delta^{57}\text{Fe}$  values give unclear indications about the relation to the preserved metal.

### Oxygen isotopes

The corrosion products of SM9.99.242 and the water from the Mediterranean Sea in this region have virtually the same O isotope composition ( $\delta^{18}\text{O}_{\text{seawater}} = +1.12\text{‰}$  (de Montety et al. 2008)). The depth from which the water sample was taken

is unknown, but according to depth profiles from other areas of the Mediterranean Sea and especially from the Gulf of Lion (Pierre 1999), depth-dependent variation is negligible within 50 m below the surface. Despite its location in the Rhône river delta about 2 km away from the modern-day coast, a mixture of seawater and Rhône river water seems very unlikely: the site of SM9 lies in between the plumes of two tributaries (Gangloff et al. 2017; Many et al. 2018) and the aquifer becomes saline several kilometres onshore (de Montety et al. 2008).

Two possibilities exist to reach an O isotope composition of corrosion products equal to the O isotope composition of the seawater: One is when the equilibrium between water and the reaction product is not attained, and another, where the contrary is the case. The first possibility requires high photosynthetic activity with negligible respiration. This will result in DMO derived almost entirely from photosynthesis. Because O isotopes are not fractionated by photosynthesis (Guy et al. 1993), the DMO and the water will have the same O isotope composition and so will the corrosion products. This scenario would also require that the oxidation of water to hydroxide does not go along with any significant oxygen isotope fractionation.

Admittedly, this scenario seems unlikely, as there must be also considerable respiration, when photosynthetic activity is high. Additionally, DMO from the dissolution of atmospheric oxygen into the seawater has to be taken into account. As soon as respiration contributes to the O isotope composition of DMO, it will be enriched in the lighter isotope compared with seawater (Hendricks et al. 2005) and hence photosynthetically derived DMO. Dissolution of atmospheric oxygen in the seawater will shift the O isotope composition of DMO in the same direction (Wassenaar and Hendry 2007; Mader et al. 2017). Therefore, at some point during the corrosion process, oxygen isotopes in the Fe hydroxides or in akaganeite must be fractionated and this fractionation results in the same O isotopic composition than the seawater has.

Xu et al. (2002) report an enrichment of about 5.5‰ at 25°C of the heavier isotope in akaganeite compared with water in isotopic equilibrium. However, it is difficult to avoid O isotope fractionation during sample preparation, e.g. through evaporation (Bao and Koch 1999; Friedrich et al. 2015). The fractionation factor of about 1.0‰ at 25 °C reported by Bao and Koch (1999) seems more reliable. On the one hand, they are aware of these difficulties and admit that even their observed fractionation might be altered by these processes. On the other hand, such a small fractionation fits well with the very small fractionation factor observed between the structurally similar goethite and water (Bao and Koch 1999; Friedrich et al. 2015). Additionally, an increasing chloride content seems to decrease the O isotope fractionation between akaganeite and water (Yapp 2007). Thus, it seems plausible that akaganeite has the same O isotope composition once isotopic equilibrium is (mostly) attained.

If it is accepted that akaganeite behaves similarly to goethite concerning O isotope fractionation with water, isotopic equilibrium between both phases should be attained similarly fast (Friedrich et al. 2015) and no fractionation should occur after full crystallisation (Bao and Koch 1999). For this equilibrium scenario, it could then be assumed that the akaganeite bears the O isotope composition of the water it crystallised in. As this is only one object, this is far from being conclusive. Further studies will have to show, if this holds true for e.g. magnetite as corrosion product.

## Terrestrial corrosion

### Iron isotopes

The ore specimen shows a heterogeneous composition within the ore and a significant enrichment of the lighter isotopes on its surface. The heterogeneous composition of the ore might be induced by postgenetic hydrothermal fluids cross-cutting the ore (Markl et al. 2006), as indicated by veins filled with gangue minerals (Fig. 2) (Rose et al. 2019). This phenomenon will not be discussed here, as it is unrelated to surface processes.

The enrichment of the lighter isotopes on the surface of the ore specimen must be regarded as direct consequence of weathering processes. The presence of isotopically lighter Fe (hydr)oxides, such as goethite, as precipitation products is in accordance with results reported in the literature (Skulan et al. 2002; Wiederhold et al. 2007; Kiczka et al. 2011). Two possibilities for the preceding surficial dissolution of Fe oxides from the ore exist: the preferential dissolution of isotopically light Fe, and the dissolution of Fe oxides without isotope fractionation followed by the precipitation of isotopically lighter Fe (hydr)oxides and loss of the isotopically heavier dissolved Fe. Based on mass balance calculations, Yesavage et al. (2012) concluded that Fe isotope fractionation occurring during weathering of shale can be explained best with a negligible Fe isotope fractionation during dissolution and the precipitation of isotopically lighter Fe (hydr)oxides. This model corresponds to the latter of the two outlined scenarios for the data of the ore specimen. Li et al. (2017) came to the same result concerning the dissolution of iron, since they observed significant Fe loss but only very limited fractionation during laterite formation. Additionally, it cannot be ruled out that the small fractionation observed by them was induced by interaction with organic matter. As a result, it is concluded that similar to the model presented by Yesavage et al. (2012), Fe isotope fractionation during the dissolution of Fe from the ore seems negligibly small and that the isotopically heavier dissolved Fe is lost to the soil water.

For the two analysed iron objects, Fe isotope fractionation seems to be absent during corrosion under oxidising conditions. Only one sample of KS-Fe, taken from the blistered corrosion, displays a heavier isotope composition compared with the other

samples of this specimen. Such an enrichment in heavier isotopes can be explained by the presence of organic material, on which isotopically heavy Fe preferentially adsorbs (Brantley et al. 2001; Beard et al. 2010; Ilina et al. 2013; Lotfi-Kalahroodi et al. 2019; Rose et al. 2019). Additional to our objects, Milot et al. (2016) analysed atmospheric corrosion products from one semi-product and report Fe isotope compositions indistinguishable from the metallic core. However, this object will not be included in the discussion as it represents atmospheric corrosion on an object from a marine burial environment and the corrosion most likely occurred in direct interaction with the atmosphere after its recovery.

These observations are substantiated by current knowledge about Fe isotope fractionation, which can occur at two different steps during corrosion: dissolution of the Fe from the metal and precipitation of the corrosion products. As was shown above, dissolution of Fe phases seems not to cause isotope fractionation (Li et al. 2017; Yesavage et al. 2012) but fractionation might occur afterwards by complexation with e.g. organic matter and loss of dissolved Fe (Fantle and DePaolo 2004; Wiederhold et al. 2007). Because in both cases the presence of goethite indicate a sufficiently oxidising atmosphere, changes in the redox conditions should have negligible impact on the fractionation of Fe isotopes during the dissolution of Fe (Schuth et al. 2015). Although the solubility of Fe (hydr)oxides is sufficiently high to expect loss of Fe into soil water as in the case of the ore specimen, no significant loss of Fe seems to occur after dissolution during corrosion of iron objects (Neff et al. 2006). Consequently, the Fe isotopic composition of the corrosion product will be consistent with that of the initial metal, which is in agreement with all present analytical data.

No insight could be gained from the available data for Fe isotope fractionation processes on the micro- or nano-scale. During Fe corrosion, dissolved Fe ions move away from the metal-electrolyte interface. As soon as oxidising conditions are reached, they rapidly precipitate as Fe (hydr)oxides in pores and fractures of existing corrosion products (Neff et al. 2005, 2006). During these reactions, Fe isotope fractionation occurs. For instance, the corrosion products of MG-Fe are goethite and magnetite/maghemite. While goethite preferentially incorporates the lighter isotopes (Skulan et al. 2002; Wiederhold et al. 2007; Kiczka et al. 2011) and might later have the same isotopic composition like the dissolved Fe due to a complex exchange mechanism (Friedrich et al. 2015; Jang et al. 2008; Reddy et al. 2015), magnetite becomes enriched in the heavier isotopes compared to aqueous Fe(II) (Friedrich et al. 2014a). For maghemite, respective studies are lacking. The presence of goethite indicates oxidising conditions, whereas the presence of magnetite/maghemite indicates lower levels of oxygen. They might result from the removal of molecular oxygen by the decay of organic material in the compost bin but also from the limited diffusion of molecular oxygen from the atmosphere through the overlying corrosion products. Goethite and

magnetite show opposite Fe isotope fractionation trends during their formation; hence, heterogeneous Fe isotope compositions within the corrosion layer are expected. Cracking and flaking, emerging from drying and the growth of the corrosion products, locally change the availability of molecular oxygen and water within the corrosion layer. The result is a complex growth pattern of both phases and hence an equally complex pattern of different Fe isotope compositions.

### Oxygen isotopes

The O isotope compositions of the corrosion products from MG-Fe and KS-Fe show a strong enrichment of  $^{18}\text{O}$  compared with the local precipitation and groundwater. Like the Fe isotope data of MG-Fe, the O isotope data displays a mixture of goethite and magnetite/maghemite. MG-Fe is approximately 8‰ heavier in its O isotopic composition compared with Munich groundwater (−11.5 to −10.5‰ (Förstel and Hütten 1983)) and Munich rain (−10.6 to −10.0‰ (Tütken et al. 2004)), whereas KS-Fe shows a much bigger offset of around 17‰ (groundwater −7.5 to −8.5‰ (Förstel and Hütten 1983), rain −7.5 to −8.1‰ (Tütken et al. 2004)).

The O isotope composition of the water interacting with the artefacts is significantly altered by evaporation outside of water-logged environments, resulting in a shift towards less negative  $\delta^{18}\text{O}$ -values (Bao et al. 2000; Yapp 2008). For both artefacts, the burial location was favourable for evaporation; hence, the water interacting with the artefacts can be assumed to be isotopically heavier than the precipitation. Oxygen might be further isotopically fractionated during its incorporation from the water into the corrosion products. The difference between goethite and the coexisting water seems to be negligibly small (Bao et al. 2000; Friedrich et al. 2015). As was shown for marine corrosion, the formation of magnetite should enrich  $^{16}\text{O}$  in the corrosion product. Studies investigating O isotope fractionation of maghemite are lacking.

Beside water, DMO is the other source of oxygen for corrosion products and its isotopic composition in the soil gas is controlled by a complex interplay between diffusion and respiration (Aggarwal and Dillon 1998; Angert et al. 2001). The dissolution of DMO from the soil gas into the soil water results in a slight enrichment of the heavier isotope in the soil fluid's DMO (Mader et al. 2017). And finally, a possible depletion of  $^{16}\text{O}$  in the DMO during the oxidation of Fe hydroxides must be taken into account (Oba and Poulson 2009).

All these processes were proceeding during the corrosion of the artefacts. For some, like the isotope fractionation between water and the corrosion products, differences between both sites can be regarded as negligible to the large overall fractionation between the reservoirs and the corrosion products. Evaporation and respiration seem to be the major causes of the observed O isotope fractionations. Although their relative contribution to the observed overall O isotope fractionation cannot be

quantified with the available data, differences between them most likely cause the difference in the O isotope fractionation on both sites. Evaporation alone is easy to fractionate the O isotopes of the soil water sufficiently (Luz et al. 2009). It will have had a more pronounced effect on KS-Fe than on MG-Fe. KS-Fe was shallowly buried in a well-drained sand soil with nearly no vegetation. The sun was able to shine directly on it for a prolonged period. In contrast to this, MG-Fe was located in contact with a humus-rich soil/compost amid high grass plants under a walnut tree, hence with significantly reduced evaporation compared with KS-Fe. Additionally, respiration might have had a much stronger effect on the DMO's O isotopic composition at KS-Fe than on the one at MG-Fe as the latter was in close contact with the atmosphere. This would have led to a rapid exchange between the isotopically heavier respired soil gas and unrespired oxygen. As a result, the DMO interacting with KS-Fe might have had a heavier O isotope composition than the DMO at MG-Fe.

A possible explanation for the difference in the O isotope composition of KS-Fe between the heavier inner layer and the lighter outer layer might be the depletion of the lighter O isotopes during the diffusion of DMO through the corrosion layer. DMO diffusing into the corrosion layer will react with dissolved Fe hydroxides diffusing outward (Neff et al. 2005, 2006) and as this reaction might preferentially remove the lighter O isotope from the DMO (Oba and Poulson 2009), it becomes increasingly isotopically heavy until it reaches the inner layer.

### Potential applications in archaeometallurgy

Despite the limited number of objects analysed and the restricted data on Fe and O isotope fractionation during iron corrosion, some preliminary suggestions for applications in archaeometallurgy can be provided. The small or even absent alteration of the O isotope composition by natural processes after precipitation of Fe (hydr)oxides (Yapp 1997; Poage et al. 2000; Sjöström et al. 2004; Friedrich et al. 2015) may lead one to expect some kind of temperature or time record within the corrosion products. However, the data presented here show no or only little potential for the application of the O isotope signatures to iron corrosion products. Generally spoken, it seems that corrosion products show the O isotope composition of the source water. Most of the processes which determine the O isotope composition of the source water are controlled by the local environmental conditions, particularly evaporation and respiration. Quantification of the contribution of the various processes to the overall isotope signature is extremely difficult if not impossible.

In marine environments, the source water usually is seawater, in which the artefact is submerged. But so far, this was shown for only one example, so that there is the need for larger and specifically designed studies.

In contrast to O isotopes, the behaviour of Fe isotopes bears some potential. Bulk isotope analysis of the corrosion layer allows the determination of the Fe isotopic composition of an object. Admittedly, variations of the Fe isotope compositions within the corrosion layers might be present on the micro-scale and due to dissolution processes, the outer surface of the corrosion might have a different isotopic composition compared with the bulk of the sample. But the only hint to such isotopic heterogeneities is sample KS-Fe2, which is likely to be affected by a high content of organic carbon (see above). In all other cases, around 1 mg of sample was enough to yield the same Fe isotope composition like the metal. Consequently, direct sampling and thus damaging of the object might be avoidable, which in turn might strongly facilitate access to iron artefacts for analysis and opens up the possibility for large-scale studies of iron objects once applications of Fe isotopes in archaeometallurgy are advanced (Milot 2016; Milot et al. 2016; Rose et al. 2019). Although the discriminatory power of Fe isotopes seems to be low for provenance studies and the number of analysed ore deposits is small, it was shown that certain types of deposits might be discriminated with Fe isotopes. Although the information obtained from Fe isotopes might tell little about the object, this might still be worthwhile if the object is otherwise inaccessible at all.

Admittedly, the conclusions concerning Fe isotope applications cannot be transferred directly from oxidising soil environments to acidic or anoxic soils. Corrosion products in these environments are similar to marine corrosion, as they might lead to the formation of a protective corrosion layer of magnetite or siderite (Saheb et al. 2010; Michelin et al. 2013). Solubility of Fe is much higher in acidic and anoxic soils and can result in significant loss of Fe (Gerwin and Baumhauer 2000) before such a protective layer is established. Consequently, it might not be possible to establish a direct relationship between the Fe isotopic composition of the metal and the corrosion products in those cases. Likewise, it must remain open at this point what happens when the burial conditions change dramatically.

## Conclusions

This study determined the Fe and O isotope compositions of the corrosion layer of iron artefacts and constitutes a first attempt to extract information about the artefact from the corrosion layer, i.e. without sampling the artefact itself. Two artefacts from oxidising environments above the water table and one artefact from a submerged Roman shipwreck as an example for marine corrosion were analysed.

O isotope fractionation among the corrosion products and the reservoirs of molecular oxygen and water was successfully traced for all artefacts, but it cannot be assigned to specific parameters. In all objects, the corrosion products seem to bear

the O isotope composition of their source water. But too many parameters influence the O isotope composition of the source water in oxidising environments above the water table, with the most important of them controlled by the local environment. In marine environments, the source water is the surrounding water and further studies are needed to support the observations made on a single object in this study. At the present state, it seems unlikely that O isotope signatures of corrosion products will be of relevance for archaeometallurgical research.

No Fe isotope fractionation was observed in the metal objects. This either indicates that no loss of dissolved Fe occurred during corrosion in oxidizing environments or that all involved processes in the end isotopically balances losses and gains of Fe during interaction with the environment. Based on the present data, neither the one nor the other can be excluded. Comparison with literature data for objects buried in seawater revealed a possible influence of the concentration of dissolved molecular oxygen in the water on the Fe isotope composition of the corrosion products. Consequently, Fe isotope composition of iron objects, which were deposited in oxidising environments, can be determined in the corrosion layer by bulk sampling (~1 mg). Thus, they represent a similarity of Fe isotope composition with the original and uncorroded iron metal without any need for invasive sampling. This opens up the possibility for Fe isotope analysis of precious artefacts unavailable for direct sampling. Future studies have to address to what extent this holds true for reducing conditions, such as in marine environments or anoxic soils, and for dramatic changes in the burial environment. At the same time, isotopic homogeneity in the corrosion layer might not be present on the micro-scale and might offer information about the burial conditions and their changes over time.

**Acknowledgements** The Hermann-Willkomm-Stiftung thankfully financially supported the stay of T. Rose in Lyon. Luc Long (Marseille) graciously allowed us to sample and analyse the Roman semi-product SM9.99.242. T. Rose is grateful for the support of Guntram Gassmann during fieldwork. We thank Katrin Westner, Eveline Salzmann, and Chiara Giroto for fruitful discussions on an earlier draft of the article and improvement of the language. We are grateful for the comments of the two reviewers, which improved the article considerably.

**Funding information** The Institut für Geowissenschaften of the Goethe Universität Frankfurt and the Deutsches Bergbau-Museum Bochum are thanked for funding the analytical work of Thomas Rose's Master thesis. FIERCE is financially supported by the Wilhelm and Else Heraeus Foundation and by the Deutsche Forschungsgemeinschaft (DFG, INST 161/921-1 FUGG and INST 161/923-1 FUGG), which is gratefully acknowledged. This is FIERCE contribution no. 22.

## References

Aggarwal PK, Dillon MA (1998) Stable isotope composition of molecular oxygen in soil gas and groundwater: a potentially robust tracer

- for diffusion and oxygen consumption processes. *Geochim Cosmochim Acta* 62:577–584. [https://doi.org/10.1016/S0016-7037\(97\)00377-3](https://doi.org/10.1016/S0016-7037(97)00377-3)
- Albarède F, Télouk P, Lamboux A et al (2011) Isotopic evidence of unaccounted for Fe and Cu erythropoietic pathways. *Metallomics* 3:926–933. <https://doi.org/10.1039/c1mt00025j>
- Angert A, Luz B, Yakir D (2001) Fractionation of oxygen isotopes by respiration and diffusion in soils and its implications for the isotopic composition of atmospheric O<sub>2</sub>. *Glob Biogeochem Cycles* 15:871–880. <https://doi.org/10.1029/2000GB001371>
- Balter V, Lamboux A, Zazzo A, Télouk P, Leverrier Y, Marvel J, Moloney AP, Monahan FJ, Schmidt O, Albarède F (2013) Contrasting Cu, Fe, and Zn isotopic patterns in organs and body fluids of mice and sheep, with emphasis on cellular fractionation. *Metallomics* 5:1470–1482. <https://doi.org/10.1039/c3mt00151b>
- Bao H, Koch PL (1999) Oxygen isotope fractionation in ferric oxide-water systems: low temperature synthesis. *Geochim Cosmochim Acta* 63:599–613. [https://doi.org/10.1016/S0016-7037\(99\)00005-8](https://doi.org/10.1016/S0016-7037(99)00005-8)
- Bao H, Koch PL, Thiemens MH (2000) Oxygen isotopic composition of ferric oxides from recent soil, hydrologic, and marine environments. *Geochim Cosmochim Acta* 64:2221–2231. [https://doi.org/10.1016/S0016-7037\(00\)00351-3](https://doi.org/10.1016/S0016-7037(00)00351-3)
- Baron S, Coustures M-P, Béziat D, Guérin M, Huez J, Robbiola L (2011) Lingots de plomb et barres de fer des épaves romaines des Saintes-Maries-de-la-Mer (Bouches-du-Rhône, France): Questions de traçabilité comparée. *Revue Archéologique de Narbonnaise* 44: 71–98
- Beard BL, Handler RM, Scherer MM, Wu L, Czaja AD, Heimann A, Johnson CM (2010) Iron isotope fractionation between aqueous ferrous iron and goethite. *Earth Planet Sci Lett* 295:241–250. <https://doi.org/10.1016/j.epsl.2010.04.006>
- Bellot-Gurlet L, Neff D, Réguer S, Monnier J, Saheb M, Dillmann P (2009) Raman studies of corrosion layers formed on archaeological irons in various media. *J Nano Res* 8:147–156. <https://doi.org/10.4028/www.scientific.net/JNanoR.8.147>
- Benson BB, Krause D (1984) The concentration and isotopic fractionation of oxygen dissolved in freshwater and seawater in equilibrium with the atmosphere. *Limnol Oceanogr* 29:620–632. <https://doi.org/10.4319/lo.1984.29.3.0620>
- Blakelock E, Martín-Torres M, Veldhuijzen HA, Young T (2009) Slag inclusions in iron objects and the quest for provenance: an experiment and a case study. *J Archaeol Sci* 36:1745–1757. <https://doi.org/10.1016/j.jas.2009.03.032>
- Blanchard M, Dauphas N, Hu MY, Roskosz M, Alp EE, Golden DC, Sio CK, Tissot FLH, Zhao J, Gao L, Morris RV, Fornace M, Floris A, Lazzeri M, Balan E (2015) Reduced partition function ratios of iron and oxygen in goethite. *Geochim Cosmochim Acta* 151:19–33. <https://doi.org/10.1016/j.gca.2014.12.006>
- Brand WA, Coplen TB, Vogl J, Rosner M, Prohaska T (2014) Assessment of international reference materials for isotope-ratio analysis (IUPAC technical report). *Pure Appl Chem* 86:425–467. <https://doi.org/10.1515/pac-2013-1023>
- Brantley SL, Liermann LJ, Bullen TD (2001) Fractionation of Fe isotopes by soil microbes and organic acids. *Geology* 29:535. [https://doi.org/10.1130/0091-7613\(2001\)029<0535:FOFIBS>2.0.CO;2](https://doi.org/10.1130/0091-7613(2001)029<0535:FOFIBS>2.0.CO;2)
- Brauns M, Schwab R, Gassmann G, Wieland G, Pernicka E (2013) Provenance of Iron age iron in southern Germany: a new approach. *J Archaeol Sci* 40:841–849. <https://doi.org/10.1016/j.jas.2012.08.044>
- Brauns M, Yahalom-Mack N, Stepanov I, Sauder L, Keen J, Eliyahu-Behar A (2020) Osmium isotope analysis as an innovative tool for provenancing ancient iron: a systematic approach. *PLoS One* 15:e0229623. <https://doi.org/10.1371/journal.pone.0229623>
- Charlton MF (2015) The last frontier in ‘sourcing’: the hopes, constraints and future for iron provenance research. *J Archaeol Sci* 56:210–220. <https://doi.org/10.1016/j.jas.2015.02.017>
- Coustures M-P, Béziat D, Tollon F, Domergue C, Long L, Rebiscoul A (2003) The use of trace element analysis of entrapped slag inclusions to establish ore – bar iron links: examples from two gallo-roman iron-making sites in France (Les Martyrs, Montagne Noire, and Les Ferrys, Loiret). *Archaeometry* 45:599–613. <https://doi.org/10.1046/j.1475-4754.2003.00131.x>
- Craddock PR, Dauphas N (2011) Iron isotopic compositions of geological reference materials and chondrites. *Geostand Geoanal Res* 35: 101–123. <https://doi.org/10.1111/j.1751-908X.2010.00085.x>
- Desaulty A-M, Dillmann P, L’Héritier M, Mariet C, Gratuze B, Joron J-L, Fluzin P (2009) Does it come from the Pays de Bray?: examination of an origin hypothesis for the ferrous reinforcements used in French medieval churches using major and trace element analyses. *J Archaeol Sci* 36:2445–2462. <https://doi.org/10.1016/j.jas.2009.07.002>
- Dillmann P, L’Héritier M (2007) Slag inclusion analyses for studying ferrous alloys employed in French medieval buildings: supply of materials and diffusion of smelting processes. *J Archaeol Sci* 34: 1810–1823. <https://doi.org/10.1016/j.jas.2006.12.022>
- Dillmann P, Schwab R, Bauvais S, Brauns M, Disser A, Leroy S, Gassmann G, Fluzin P (2017) Circulation of iron products in the North-Alpine area during the end of the first Iron Age (6 th –5 th c. BC): a combination of chemical and isotopic approaches. *J Archaeol Sci* 87:108–124. <https://doi.org/10.1016/j.jas.2017.10.002>
- Downs RT, Hall-Wallace M (2003) The American mineralogist crystal structure database. *Am Mineral* 88:247–250
- Fantle MS, DePaolo DJ (2004) Iron isotopic fractionation during continental weathering. *EPSL* 228:547–562. <https://doi.org/10.1016/j.epsl.2004.10.013>
- Förstel H, Hütten H (1983) Oxygen isotope ratios in German groundwater. *Nature* 304:614–616. <https://doi.org/10.1038/304614a0>
- Friedrich AJ, Beard BL, Reddy TR, Scherer MM, Johnson CM (2014a) Iron isotope fractionation between aqueous Fe(II) and goethite revisited: new insights based on a multi-direction approach to equilibrium and isotopic exchange rate modification. *Geochim Cosmochim Acta* 139:383–398. <https://doi.org/10.1016/j.gca.2014.05.001>
- Friedrich AJ, Beard BL, Rosso KM, Scherer MM, Spicuzza MJ, Valley JW, Johnson CM (2015) Low temperature, non-stoichiometric oxygen-isotope exchange coupled to Fe(II)–goethite interactions. *Geochim Cosmochim Acta* 160:38–54. <https://doi.org/10.1016/j.gca.2015.03.029>
- Friedrich AJ, Beard BL, Scherer MM, Johnson CM (2014b) Determination of the Fe(II)<sub>aq</sub>–magnetite equilibrium iron isotope fractionation factor using the three-isotope method and a multi-direction approach to equilibrium. *Earth Planet Sci Lett* 391:77–86. <https://doi.org/10.1016/j.epsl.2014.01.032>
- Gangloff A, Verney R, Doxaran D, Ody A, Estournel C (2017) Investigating Rhône River plume (Gulf Of Lions, France) dynamics using metrics analysis from the MERIS 300m Ocean Color archive (2002–2012). *Cont Shelf Res* 144:98–111. <https://doi.org/10.1016/j.csr.2017.06.024>
- Gerwin W, Baumhauer R (2000) Effect of soil parameters on the corrosion of archaeological metal finds. *Geoderma* 96:63–80. [https://doi.org/10.1016/S0016-7061\(00\)00004-5](https://doi.org/10.1016/S0016-7061(00)00004-5)
- Gorski CA, Handler RM, Beard BL, Pasakarnis T, Johnson CM, Scherer MM (2012) Fe atom exchange between aqueous Fe<sup>2+</sup> and magnetite. *Environ Sci Technol* 46:12399–12407. <https://doi.org/10.1021/es204649a>
- Guy RD, Fogel ML, Berry JA (1993) Photosynthetic fractionation of the stable isotopes of oxygen and carbon. *Plant Physiol* 101:37–47. <https://doi.org/10.1104/pp.101.1.37>
- Handler RM, Beard BL, Johnson CM, Scherer MM (2009) Atom exchange between aqueous Fe(II) and goethite: an Fe isotope tracer study. *Environ Sci Technol* 43:1102–1107. <https://doi.org/10.1021/es802402m>

- Handler RM, Friedrich AJ, Johnson CM, Rosso KM, Beard BL, Wang C, Latta DE, Neumann A, Pasakarnis T, Premaratne WAPJ, Scherer MM (2014) Fe(II)-catalyzed recrystallization of goethite revisited. *Environ Sci Technol* 48:11302–11311. <https://doi.org/10.1021/es503084u>
- Hansel CM, Benner SG, Fendorf S (2005) Competing Fe(II)-induced mineralization pathways of ferrihydrite. *Environ Sci Technol* 39:7147–7153. <https://doi.org/10.1021/es050666z>
- Hendricks MB, Bender ML, Barnett BA, Strutton P, Chavez FP (2005) Triple oxygen isotope composition of dissolved O<sub>2</sub> in the equatorial Pacific: a tracer of mixing, production, and respiration. *J Geophys Res* 110:C12021. <https://doi.org/10.1029/2004JC002735>
- IAEA (2017) Reference sheet for international measurement standards: VSMOW2 Vienna Standard Mean Ocean Water 2, water; SLAP2 Standard Light Antarctic Precipitation 2, water. [https://nucleus.iaea.org/rpst/documents/vsmow2\\_slap2.pdf](https://nucleus.iaea.org/rpst/documents/vsmow2_slap2.pdf). Accessed 16 July 2019
- Iilina SM, Poitrasson F, Lapitskiy SA, Alekhin YV, Viers J, Pokrovsky OS (2013) Extreme iron isotope fractionation between colloids and particles of boreal and temperate organic-rich waters. *Geochim Cosmochim Acta* 101:96–111. <https://doi.org/10.1016/j.gca.2012.10.023>
- Jang J-H, Mathur R, Liemann LJ, Ruebush S, Brantley SL (2008) An iron isotope signature related to electron transfer between aqueous ferrous iron and goethite. *Chem Geol* 250:40–48. <https://doi.org/10.1016/j.chemgeo.2008.02.002>
- Joosten I, Jansen J, Kars H (1998) Geochemistry and the past: estimation of the output of a Germanic iron production site in the Netherlands. *J Geochem Explor* 62:129–137. [https://doi.org/10.1016/S0375-6742\(97\)00043-5](https://doi.org/10.1016/S0375-6742(97)00043-5)
- Kiczka M, Wiederhold JG, Frommer J, Voegelin A, Kraemer SM, Bourdon B, Kretzschmar R (2011) Iron speciation and isotope fractionation during silicate weathering and soil formation in an alpine glacier forefield chronosequence. *Geochim Cosmochim Acta* 75:5559–5573. <https://doi.org/10.1016/j.gca.2011.07.008>
- Knox M, Quay PD, Wilbur D (1992) Kinetic isotopic fractionation during air-water gas transfer of O<sub>2</sub>, N<sub>2</sub>, CH<sub>4</sub>, and H<sub>2</sub>. *J Geophys Res* 97:20335. <https://doi.org/10.1029/92JC00949>
- Kroopnick P, Craig H (1972) Atmospheric oxygen: isotopic composition and solubility fractionation. *Science* 175:54–55
- Leroy S, Cohen SX, Verna C, Gratuzé B, Téreygeol F, Fluzin P, Bertrand L, Dillmann P (2012) The medieval iron market in Ariège (France). Multidisciplinary analytical approach and multivariate analyses. *J Archaeol Sci* 39:1080–1093. <https://doi.org/10.1016/j.jas.2011.11.025>
- L'Héritier M, Leroy S, Dillmann P, Gratuzé B (2016) Characterization of slag inclusions in Iron objects. In: Dussubieux L, Golitko M, Gratuzé B (eds) Recent advances in laser ablation ICP-MS for archaeology. Springer, Heidelberg, Berlin, pp 213–228
- Li B, Yeung LY, Hu H, Ash JL (2019) Kinetic and equilibrium fractionation of O<sub>2</sub> isotopologues during air-water gas transfer and implications for tracing oxygen cycling in the ocean. *Mar Chem* 210:61–71. <https://doi.org/10.1016/j.marchem.2019.02.006>
- Li M, He Y-S, Kang J-T, Yang XY, He ZW, Yu HM, Huang F (2017) Why was iron lost without significant isotope fractionation during the lateritic process in tropical environments? *Geoderma* 290:1–9. <https://doi.org/10.1016/j.geoderma.2016.12.003>
- Long L, Rico C, Domergue C (2002) Les épaves antiques de Camargue et le commerce maritime du fer en Méditerranée nord-occidentale (Ier siècle avant J.-C. - Ier siècle après J.-C.). In: Khanoussi M, Ruggeri P, Vismara C (eds) *L' Africa Romana*. Carocci, Roma, pp 161–188
- Lotfi-Kalahroodi E, Pierson-Wickmann A-C, Guénet H, Rouxel O, Ponzevera E, Bouhnik-le Coz M, Vantelon D, Dia A, Davranche M (2019) Iron isotope fractionation in iron-organic matter associations: experimental evidence using filtration and ultrafiltration. *Geochim Cosmochim Acta* 250:98–116. <https://doi.org/10.1016/j.gca.2019.01.036>
- Luz B, Barkan E, Yam R, Shemesh A (2009) Fractionation of oxygen and hydrogen isotopes in evaporating water. *Geochim Cosmochim Acta* 73:6697–6703. <https://doi.org/10.1016/j.gca.2009.08.008>
- Mader M, Schmidt C, van Geldern R, Barth JA (2017) Dissolved oxygen in water and its stable isotope effects: a review. *Chem Geol* 473:10–21. <https://doi.org/10.1016/j.chemgeo.2017.10.003>
- Mandernack KW, Bazylnski DA, Shanks WC III, Bullen TD (1999) Oxygen and Iron isotope studies of magnetite produced by magnetotactic bacteria. *Science* 285:1892–1896. <https://doi.org/10.1126/science.285.5435.1892>
- Many G, Bourrin F, Durrieu de Madron X, Ody A, Doxaran D, Cauchy P (2018) Glider and satellite monitoring of the variability of the suspended particle distribution and size in the Rhône ROFI. *Prog Oceanogr* 163:123–135. <https://doi.org/10.1016/j.pocean.2017.05.006>
- Maréchal CN, Télouk P, Albarède F (1999) Precise analysis of copper and zinc isotopic compositions by plasma-source mass spectrometry. *Chem Geol* 156:251–273. [https://doi.org/10.1016/S0009-2541\(98\)00191-0](https://doi.org/10.1016/S0009-2541(98)00191-0)
- Markl G, von Blanckenburg F, Wagner T (2006) Iron isotope fractionation during hydrothermal ore deposition and alteration. *Geochim Cosmochim Acta* 70:3011–3030. <https://doi.org/10.1016/j.gca.2006.02.028>
- Matthiesen H, Hilbert LR, Gregory DJ (2013) Siderite as a corrosion product on archaeological Iron from a waterlogged environment. *Stud Conserv* 48:183–194. <https://doi.org/10.1179/sic.2003.48.3.183>
- Memet JB (2007) The corrosion of metallic artefacts in seawater: descriptive analysis. In: Dillmann P, Béranger G, Piccardo P, Matthiesen H (eds) *Corrosion of metallic heritage artefacts*. Woodhead Publishing, Cambridge, pp 152–169
- Michelin A, Drouet E, Foy E, Dynes JJ, Neff D, Dillmann P (2013) Investigation at the nanometre scale on the corrosion mechanisms of archaeological ferrous artefacts by STXM. *J Anal At Spectrom* 28:59–66. <https://doi.org/10.1039/C2JA30250K>
- Milot J (2016) Utilisation des isotopes du fer pour le traçage des métaux anciens: développement méthodologique et applications archéologiques. PhD thesis, Université Toulouse 3 Paul Sabatier; Sciences de la Terre et des Planètes Solides
- Milot J, Poitrasson F, Baron S, Coustures M-P (2016) Iron isotopes as a potential tool for ancient iron metals tracing. *J Archaeol Sci* 76:9–20. <https://doi.org/10.1016/j.jas.2016.10.003>
- de Montety V, Radakovitch O, Vallet-Coulomb C, Blavoux B, Hermitte D, Valles V (2008) Origin of groundwater salinity and hydrogeochemical processes in a confined coastal aquifer: case of the Rhône delta (southern France). *Appl Geochem* 23:2337–2349. <https://doi.org/10.1016/j.apgeochem.2008.03.011>
- Neff D, Dillmann P, Bellot-Gurlet L, Béranger G (2005) Corrosion of iron archaeological artefacts in soil: characterisation of the corrosion system. *Corros Sci* 47:515–535. <https://doi.org/10.1016/j.corsci.2004.05.029>
- Neff D, Dillmann P, Descostes M, Béranger G (2006) Corrosion of iron archaeological artefacts in soil: estimation of the average corrosion rates involving analytical techniques and thermodynamic calculations. *Corros Sci* 48:2947–2970. <https://doi.org/10.1016/j.corsci.2005.11.013>
- Neff D, Réguer S, Bellot-Gurlet L et al (2004) Structural characterization of corrosion products on archaeological iron: an integrated analytical approach to establish corrosion forms. *J Raman Spectrosc* 35:739–745. <https://doi.org/10.1002/jrs.1130>
- North NA, Pearson C (1978) Washing methods for chloride removal from marine iron artifacts. *Stud Conserv* 23:174–186. <https://doi.org/10.1179/sic.1978.023>
- Notis MR (2002) A ghost story: remnant structures in corroded ancient iron objects. *MRS Proc* 712. <https://doi.org/10.1557/PROC-712-II.5.4>

- Oba Y, Poulson SR (2009) Oxygen isotope fractionation of dissolved oxygen during reduction by ferrous iron. *Geochim Cosmochim Acta* 73:13–24. <https://doi.org/10.1016/j.gca.2008.10.012>
- Pagès G (2008) La métallurgie du fer en France méditerranéenne de l'Antiquité au début du Moyen Âge: Jalons d'une approche interdisciplinaire. PhD thesis, Université Montpellier III - Paul Valéry; Arts et Lettres, Langues et Sciences Humaines et Sociales
- Pagès G, Long L, Fluzin P, Dillmann P (2008) Réseaux de production et standards de commercialisation du fer antique en Méditerranée: Les demi-produits des épaves romaines des Saintes-Maries-de-la-Mer (Bouches-du-Rhône). *Revue Archéologique de Narbonnaise* 41: 261–283. <https://doi.org/10.3406/ran.2008.1194>
- Park B, Dempsey BA (2005) Heterogeneous oxidation of Fe(II) on ferric oxide at neutral pH and a low partial pressure of O<sub>2</sub>. *Environ Sci Technol* 39:6494–6500. <https://doi.org/10.1021/es0501058>
- Pierre C (1999) The oxygen and carbon isotope distribution in the Mediterranean water masses. *Mar Geol* 153:41–55. [https://doi.org/10.1016/S0025-3227\(98\)00090-5](https://doi.org/10.1016/S0025-3227(98)00090-5)
- Pleiner R (2000) Iron in archaeology: the European bloomery smelters. *Archeologický Ústav; Archeologický ústav AV ČR, Praha*
- Poage MA, Sjöstrom DJ, Goldberg J, Chamberlain CP, Furniss G (2000) Isotopic evidence for Holocene climate change in the northern Rockies from a goethite-rich ferricrete chronosequence. *Chem Geol* 166:327–340. [https://doi.org/10.1016/S0009-2541\(99\)00220-X](https://doi.org/10.1016/S0009-2541(99)00220-X)
- Poitrasson F, Levasseur S, Teutsch N (2005) Significance of iron isotope mineral fractionation in pallasites and iron meteorites for the core-mantle differentiation of terrestrial planets. *Earth Planet Sci Lett* 234:151–164. <https://doi.org/10.1016/j.epsl.2005.02.010>
- Poulson RL, Johnson CM, Beard BL (2005) Iron isotope exchange kinetics at the nanoparticulate ferrihydrite surface. *Am Mineral* 90: 758–763. <https://doi.org/10.2138/am.2005.1802>
- R Core Team (2017) R: a language and environment for statistical computing
- Reddy TR, Friedrich AJ, Beard BL, Johnson CM (2015) The effect of pH on stable iron isotope exchange and fractionation between aqueous Fe(II) and goethite. *Chem Geol* 397:118–127. <https://doi.org/10.1016/j.chemgeo.2015.01.018>
- Réguer S, Dillmann P, Mirambet F et al (2006) Investigation of Cl corrosion products of iron archaeological artefacts using micro-focused synchrotron X-ray absorption spectroscopy. *Appl Phys A* 83:189–193. <https://doi.org/10.1007/s00339-006-3506-3>
- Réguer S, Neff D, Bellot-Gurlet L, Dillmann P (2007) Deterioration of iron archaeological artefacts: micro-Raman investigation on Cl-containing corrosion products. *J Raman Spectrosc* 38:389–397. <https://doi.org/10.1002/jrs.1659>
- Rémazeilles C, Refait P (2007) On the formation of  $\beta$ -FeOOH (akaganéite) in chloride-containing environments. *Corros Sci* 49: 844–857. <https://doi.org/10.1016/j.corsci.2006.06.003>
- Rimmer M, Watkinson D, Wang Q (2013) The efficiency of chloride extraction from archaeological iron objects using deoxygenated alkaline solutions. *Stud Conserv* 57:29–41. <https://doi.org/10.1179/2047058411Y.0000000005>
- Rose T, Télouk P, Klein S, Marschall HR (2019) Questioning Fe isotopes as a provenance tool: insights from bog iron ores and alternative applications in archeometry. *J Archaeol Sci* 101:52–62. <https://doi.org/10.1016/j.jas.2018.11.005>
- Saheb M, Descostes M, Neff D, Matthies H, Michelin A, Dillmann P (2010) Iron corrosion in an anoxic soil: comparison between thermodynamic modelling and ferrous archaeological artefacts characterised along with the local in situ geochemical conditions. *Appl Geochem* 25:1937–1948. <https://doi.org/10.1016/j.apgeochem.2010.10.010>
- Schuth S, Hurraß J, Munker C, Mansfeldt T (2015) Redox-dependent fractionation of iron isotopes in suspensions of a groundwater-influenced soil. *Chem Geol* 392:74–86. <https://doi.org/10.1016/j.chemgeo.2014.11.007>
- Selwyn LS, Argyropoulos V (2013) Removal of chloride and iron ions from archaeological wrought iron with sodium hydroxide and ethylenediamine solutions. *Stud Conserv* 50:81–100. <https://doi.org/10.1179/sic.2005.50.2.81>
- Selwyn LS, Sirois PI, Argyropoulos V (1999) The corrosion of excavated archaeological iron with details on weeping and akaganéite. *Stud Conserv* 44:217–232. <https://doi.org/10.1179/sic.1999.44.4.217>
- Sjöstrom DJ, Hren MT, Chamberlain CP (2004) Oxygen isotope records of goethite from ferricrete deposits indicate regionally varying holocene climate change in the Rocky Mountain region, U.S.a. *Quat Res* 61:64–71. <https://doi.org/10.1016/j.yqres.2003.08.008>
- Skulan JL, Beard BL, Johnson CM (2002) Kinetic and equilibrium Fe isotope fractionation between aqueous Fe(III) and hematite. *Geochim Cosmochim Acta* 66:2995–3015. [https://doi.org/10.1016/S0016-7037\(02\)00902-X](https://doi.org/10.1016/S0016-7037(02)00902-X)
- Sossi PA, Halverson GP, Nebel O, Eggins SM (2015) Combined separation of Cu, Fe and Zn from rock matrices and improved analytical protocols for stable isotope determination. *Geostand Geoanal Res* 39:129–149. <https://doi.org/10.1111/j.1751-908X.2014.00298.x>
- Ståhl K, Nielsen K, Jiang J, Lebeck B, Hanson JC, Norby P, van Lanschot J (2003) On the akaganéite crystal structure, phase transformations and possible role in post-excavational corrosion of iron artifacts. *Corros Sci* 45:2563–2575. [https://doi.org/10.1016/S0010-938X\(03\)00078-7](https://doi.org/10.1016/S0010-938X(03)00078-7)
- Stepanov I, Weeks L, Franke K, Cable C, Overlaet B, Magee P, Händel M, Aali YYA, Radwan MB, Zein H (2018) Methodologies for the investigation of corroded iron objects: examples from prehistoric sites in South-Eastern Arabia and Western Iran. *STAR: Sci Technol Archaeol Res* 3:270–284. <https://doi.org/10.1080/20548923.2018.1424304>
- Taylor PDP, Maeck R, de Bièvre P (1992) Determination of the absolute isotopic composition and atomic weight of a reference sample of natural iron. *Int J Mass Spectrom Ion Process* 121:111–125. [https://doi.org/10.1016/0168-1176\(92\)80075-C](https://doi.org/10.1016/0168-1176(92)80075-C)
- Toby BH, von Dreele RB (2013) GSAS-II: the genesis of a modern open-source all purpose crystallography software package. *J Appl Crystallogr* 46:544–549. <https://doi.org/10.1107/S0021889813003531>
- Tütken T, Vennemann TW, Pfretzschner H-U (2004) Analyse stabiler und radiogener Isotope in archäologischem Skelettmaterial: Herkunftsbestimmung des karolingischen Maultiers von Frankenthal und Vergleich mit spätpleistozänen Großsäugerknochen aus den Rheinablagerungen. *Prähistorische Zeitschrift* 79:89–110. <https://doi.org/10.1515/prhz.79.1.89>
- Valley JW, Kitchen N, Kohn MJ, Niendorf CR, Spicuzza MJ (1995) UWG-2, a garnet standard for oxygen isotope ratios: strategies for high precision and accuracy with laser heating. *Geochim Cosmochim Acta* 59:5223–5231. [https://doi.org/10.1016/0016-7037\(95\)00386-X](https://doi.org/10.1016/0016-7037(95)00386-X)
- Wassenaar LI, Hendry MJ (2007) Dynamics and stable isotope composition of gaseous and dissolved oxygen. *Ground Water* 45:447–460. <https://doi.org/10.1111/j.1745-6584.2007.00328.x>
- Welch SA, Beard BL, Johnson CM, Braterman PS (2003) Kinetic and equilibrium Fe isotope fractionation between aqueous Fe(II) and Fe(III). *Geochim Cosmochim Acta* 67:4231–4250. [https://doi.org/10.1016/S0016-7037\(03\)00266-7](https://doi.org/10.1016/S0016-7037(03)00266-7)
- Weyer S, Schwieters JB (2003) High precision Fe isotope measurements with high mass resolution MC-ICPMS. *Int J Mass Spectrom* 226: 355–368. [https://doi.org/10.1016/S1387-3806\(03\)00078-2](https://doi.org/10.1016/S1387-3806(03)00078-2)
- Wiederhold JG, Teutsch N, Kraemer SM, Halliday AN, Kretzschmar R (2007) Iron isotope fractionation in oxic soils by mineral weathering and podzolization. *Geochim Cosmochim Acta* 71:5821–5833. <https://doi.org/10.1016/j.gca.2007.07.023>

- Wu L, Beard BL, Roden EE, Johnson CM (2011) Stable iron isotope fractionation between aqueous Fe(II) and hydrous ferric oxide. *Environ Sci Technol* 45:1847–1852. <https://doi.org/10.1021/es103171x>
- Xu BL, Zhou GT, Zheng YF (2002) An experimental study of oxygen isotope fractionations in the goethite-akaganeite-water systems at low temperatures (in Chinese). *Geochimica* 31:366–374
- Yapp CJ (1987) Oxygen and hydrogen isotope variations among goethites ( $\alpha$ -FeOOH) and the determination of paleotemperatures. *Geochim Cosmochim Acta* 51:355–364. [https://doi.org/10.1016/0016-7037\(87\)90247-X](https://doi.org/10.1016/0016-7037(87)90247-X)
- Yapp CJ (1990) Oxygen isotopes in iron (III) oxides: 1. Mineral–water fractionation factors *Chemical Geology* 85:329–335. doi: [https://doi.org/10.1016/0009-2541\(90\)90011-U](https://doi.org/10.1016/0009-2541(90)90011-U)
- Yapp CJ (2008)  $^{18}\text{O}/^{16}\text{O}$  and D/H in goethite from a North American Oxisol of the early Eocene climatic optimum. *Geochim Cosmochim Acta* 72:5838–5851. <https://doi.org/10.1016/j.gca.2008.09.002>
- Yapp CJ (2001) Rusty relics of earth history: iron(III) oxides, isotopes, and surficial environments. *Annu Rev Earth Planet Sci* 29:165–199. <https://doi.org/10.1146/annurev.earth.29.1.165>
- Yapp CJ (2007) Oxygen isotopes in synthetic goethite and a model for the apparent pH dependence of goethite–water  $^{18}\text{O}/^{16}\text{O}$  fractionation. *Geochim Cosmochim Acta* 71:1115–1129. <https://doi.org/10.1016/j.gca.2006.11.029>
- Yapp CJ (2012) Oxygen isotope effects associated with substitution of Al for Fe in synthetic goethite: some experimental evidence and the criterion of oxygen yield. *Geochim Cosmochim Acta* 97:200–212. <https://doi.org/10.1016/j.gca.2012.09.007>
- Yapp CJ (1997) An assessment of isotopic equilibrium in goethites from a bog iron deposit and a lateritic regolith. *Chem Geol* 135:159–171. [https://doi.org/10.1016/S0009-2541\(96\)00112-X](https://doi.org/10.1016/S0009-2541(96)00112-X)
- Yesavage T, Fantle MS, Vervoort J, Mathur R, Jin L, Liermann LJ, Brantley SL (2012) Fe cycling in the Shale Hills Critical Zone Observatory, Pennsylvania: an analysis of biogeochemical weathering and Fe isotope fractionation. *Geochim Cosmochim Acta* 99:18–38. <https://doi.org/10.1016/j.gca.2012.09.029>

**Publisher's note** Springer Nature remains neutral with regard to jurisdictional claims in published maps and institutional affiliations.